Density correlation in liquid surfaces: Bedeaux-Weeks high order terms and non capillary wave background

Jose Hernández-Muñoz,[1] Enrique Chacón,[2] and Pedro Tarazona[3,a)]
[1]*Departamento de Física Teórica de la Materia Condensada, IFIMAC Condensed Matter Physics Center, Universidad Autónoma de Madrid, Madrid 28049, Spain*
[2]*Instituto de Ciencia de Materiales de Madrid, Consejo Superior de Investigaciones Científicas, Madrid 28049, Spain*
[3]*Departamento de Física Teórica de la Materia Condensada, IFIMAC Condensed Matter Physics Center, and Instituto Nicolás Cabrera de Ciencia de Materiales, Universidad Autónoma de Madrid, Madrid 28049, Spain*

(Received 26 July 2018; accepted 10 September 2018; published online 28 September 2018)

We present Molecular Dynamics (MD) simulations of liquid-vapor surfaces, and their Intrinsic Sampling Method analysis, to get a quantitative test for the theoretical prediction of the capillary wave (CW) effects on density correlation done by Bedeaux and Weeks (BW) in 1985. The results are contrasted with Wertheim's proposal which is the first term in BW series and are complemented with a (formally defined and computational accessible) proposal for the background of non-CW fluctuations. Our conclusion is that BW theory is both accurate and needed since it may differ significantly from Wertheim's proposal. We discuss the implications for the analysis of experimental X-ray surface diffraction data and MD simulations. *Published by AIP Publishing.* https://doi.org/10.1063/1.5049874

I. INTRODUCTION

Liquid surfaces are never still, capillary waves (CWs), from nanometer to macroscopic wavelengths, are unavoidable fluctuations, since the liquid phase itself depends on the balance between molecular attractions and thermal stirring set by $kT = 1/\beta$. For long wavelengths, CWs are described in terms of the surface tension γ_o, giving the thermodynamic cost for the area increase in the corrugated surface. The extension to the nanometric range is done with a wavevector dependent surface tension $\gamma(q) = \gamma_o + Kq^2 + \cdots$, to include the surface bending modulus K and possibly effects beyond it, but we have to describe how the CW spectrum ends or merges into the normal (non-CW) fluctuations in the liquid.

The Capillary Wave Theory (CWT)[1–3] was developed from the macroscopic to the mesoscopic scale. It predicts that, with the z direction across the interface, the transverse size of the system L_{xy} affects the mean density profile, formally defined as the statistical average $\rho(z) = \langle\hat{\rho}(\vec{r})\rangle$ of the density operator $\hat{\rho}(\vec{r}) = \sum_i \delta(\vec{r} - \vec{r}_i)$, with the sum over the molecular positions. However the CWT reduces the connection to the molecular scale to set an empirical top in the CW spectrum and a simple guess for an intrinsic density profile $\rho_I(z)$. That contrasts with van der Waals' view, and its modern extension in density functional (DF) theories, that describes the liquid surface in terms of a density profile $\rho_{DF}(z)$, independent of the system size and fully determined by the molecular interactions.[4]

The key concept in the CWT is the intrinsic surface (IS) which represents the instantaneous shape of the interface as $z = \xi(\vec{x}) = \sum_{\vec{q}} \xi_q e^{i\vec{q}\cdot\vec{x}}$, with Fourier components ξ_q for wavevectors $\vec{q}$ on the $\vec{x} \equiv (x, y)$ plane. The thermal fluctuations of the IS are assumed to give independent Gaussian fluctuations for each ξ_q, with mean square modulus

$$\langle|\xi_q|^2\rangle = 1/(q^2\beta\gamma(q)L_{xy}^2), \tag{1}$$

where we assume that L_{xy} is well below the capillary length (typically millimeters for simple fluids on the Earth) so that the surface fluctuations are limited by size rather than by gravity.

Assuming that the intrinsic profile $\rho_I(z)$ follows the IS corrugations, in 1976 Wertheim analyzed the CW effects on the density correlation

$$G(z, z', |\vec{x} - \vec{x'}|) \equiv \langle\hat{\rho}(\vec{r})\hat{\rho}(\vec{r}\,')\rangle - \langle\hat{\rho}(\vec{r})\rangle\langle\hat{\rho}(\vec{r}\,')\rangle, \tag{2}$$

to show the presence of long ranged correlations on the surface plane. The transverse Fourier transform of (2) should approach a $q = 0$ divergence as

$$G(z, z'; q) = \frac{\rho'(z)\rho'(z')}{q^2\beta\gamma(q)} + [\text{regular terms}], \tag{3}$$

restricted to the interfacial region by the derivative of the mean density profile.[2] The original prediction was made with γ_o, rather than with a generic function $\gamma(q)$; that amounts to treat any surface bending contribution as part of the "regular terms" which would also include any non-CW contribution to the density correlation. Over the last two decades, there has been an important effort to extract $\gamma(q)$ from X-ray diffraction experiments,[5–8] DF theories,[9–15] and computer simulations[12,16,17] based on Wertheim's prediction. The results have been confusing and puzzling, with very different predictions for $\gamma(q)$ depending on the assumptions made to represent the "regular" contributions,[4,11–16,18–21] except for their consensus for the thermodynamic limit $\gamma(0) = \gamma_o$.

a)Electronic mail: pedro.tarazona@uam.es

Soon after Wertheim's proposal, Weeks[22] pointed to higher order CW terms in $G(z, z'; q)$, which were further analyzed by Bedeaux and Weeks[23] (BW) in 1985.

The density correlation function was written as a series, $G_{\rm BW}(z, z'; q)$, of which Wertheim's $\sim q^{-2}$ term in (3) was just the first ($n = 1$) element. The validity and rigour of BW analysis within the CWT has been generally admitted but, as those authors pointed, still $G_{\rm BW}$ is not a realistic representation of (2) in a liquid surface because it fully neglects the non-CW short-ranged fluctuations both in the surface and the liquid bulk, which in (3) were thrown into the "regular terms," together with the $n \geq 2$ terms of BW series. Moreover, while in (3) $G(z, z'; q)$ depends only on $\gamma(q)$ for the same q, BW series requires the full CW spectrum, from the lowest wavevector imposed by system size to its molecular top, to predict $G_{\rm BW}(z, z'; q)$ at any q.

Some controversy on the CWT use of $\xi(\vec{x})$ and $\rho_{\rm I}(z)$ has been alive for many decades, with opponents considering that they were "mean-field concepts," absent in a rigorous statistical physics description of the interface. However, any reluctance should be wiped away by the hard fact that $\xi(\vec{x})$ and $\rho_{\rm I}(z)$ are now routinely evaluated in computer simulations, as practical tools to get a sharper molecular view of fluid interfaces. The computational procedures, such as the Intrinsic Sampling Method (ISM)[24–26] and others,[27–29] define $\xi(\vec{x})$ from the molecular positions $\{\vec{r}_i\}$ to test the CWT assumptions and to make predictions about what could be measured and computed from the more limited access to $\{\vec{r}_i\}$ obtained in experiments and DF theories. The purpose of this paper is to use the ISM to disentangle a non-CW background $G_{\rm bg}(z, z; q)$ in the density correlation (2) from the bare CW contribution $\Delta G = G - G_{\rm bg}$. The same ISM analysis provides consistently the mean square fluctuations $\langle|\xi_q|^2\rangle$, or equivalently through (1) the function $\gamma_{\rm ISM}(q)$, to be used together with the mean density profile as the molecular inputs to build the mesoscopic BW theory. Therefore, we may test directly the validity of BW series, as a representation of the bare CW contribution ΔG to the density correlation, and quantify the effect of its $n \geq 2$ terms, beyond Wertheim's prediction, for realistic simple liquid surfaces in three dimensions.

In Sec. II, we present the formal analysis for $G(z, z'; q)$ leading to BW series from CWT and to a non-CW background which includes the short-range effects of the molecular packing in the dense liquid. The Molecular Dynamics (MD) simulations are described in Sec. III, along with their ISM analysis, for two pair interaction models, the first one is the well-known Lennard-Jones (LJ) representation of simple liquids, for which we have recently presented[30] a successful comparison of the MD-ISM results with Wertheim's prediction (3). To push the test further, we use here the soft-alkali (SA) model,[31,32] a simple pair interaction designed to give the low ratio, $T_{\rm t}/T_{\rm c} = 0.10$, between the triple and critical temperatures similar to the experimental values of some liquid metals for which layered density profiles have been measured.[33,34] The results for the different contributions to $G(z, z'; q)$ are reported in Sec. IV, analyzed in terms of $\gamma(q)$, and discussed in Secs. V and VI.

II. THEORY

A. Mean and intrinsic density profiles

The CWT concepts could be formalized as a splitting in two steps for the statistical average of any magnitude A, over the full set of molecular positions $\{\vec{r}_i\}$,

$$\langle A\rangle = \left\langle \langle A\rangle_{\{\vec{r}_i\}\in[\xi]}\right\rangle_{\xi}, \tag{4}$$

where $\{\vec{r}_i\} \in [\xi]$ in the inner trace represents the statistical average over the molecular positions compatible with a fixed interfacial shape, $z = \xi(\vec{x})$, and the outer trace corresponds to the average over all the IS shapes.

$\langle A\rangle$ should be independent of that splitting, in particular, the mean density profile,

$$\rho(z) \equiv \langle\hat{\rho}(\vec{r}\,)\rangle = \langle\rho_{\rm I}[\vec{x}, z - \xi(\vec{x}); \xi]\rangle_{\xi}, \tag{5}$$

is obtained from an "intrinsic" density distribution, which is formally defined as a functional of the IS shape

$$\rho_{\rm I}[\vec{x}, z; \xi] \equiv \langle\hat{\rho}(\vec{x}, z + \xi(\vec{x}))\rangle_{\{\vec{r}_i\}\in[\xi]}, \tag{6}$$

given by the average over all the configurations compatible with that $z = \xi(\vec{x})$ and shifted to follow it. In contrast with $\rho(z)$, the intrinsic density profile defined as

$$\rho_{\rm I}(z) \equiv \langle\rho_{\rm I}[\vec{x}, z; \xi]\rangle_{\xi} \tag{7}$$

should have a well-defined large $L_{\rm xy}$ limit because of the local shift $z + \xi(\vec{x})$ used in (6). The CWT assumes that $\rho_{\rm I}[\vec{x}, z; \xi]$ is self-averaged in large enough systems, so that $\rho_{\rm I}[\vec{x}, z; \xi] \approx \rho_{\rm I}(z)$ for any instantaneous shape of the IS, and (5) leads to the usual CWT description of the surface fluctuation effects on the density profile

$$\rho(z) \approx \langle\rho_{\rm I}(z - \xi(\vec{x}))\rangle_{\xi} = \int d\xi\ \rho_{\rm I}(z - \xi)P(\xi), \tag{8}$$

with the IS average $\langle\ldots\rangle_{\xi}$ taken in terms of the probability distribution $P(\xi(\vec{x}))$, at any $\vec{x}$.

B. Bedeaux-Weeks theory for the density correlation

Wertheim,[35] Weeks,[22] and others extended (8) to a prediction for the pair distribution. Following Bedeaux and Weeks,[23] we define the CW contribution to the density correlation

$$\begin{aligned} G_{\rm BW}(z, z', \vec{x} - \vec{x}\,') &\equiv \langle\rho_{\rm I}(z - \xi(\vec{x}))\rho_{\rm I}(z' - \xi(\vec{x}'))\rangle_{\xi} \\ &\quad - \rho(z)\rho(z') \\ &= \int d\xi \int d\xi'\, \rho_{\rm I}(z - \xi)\rho_{\rm I}(z' - \xi') \\ &\quad \times P(\xi, \xi', x'') - \rho(z)\rho(z'), \end{aligned} \tag{9}$$

where $P(\xi, \xi', x'')$ is the pair height distribution at distance $x'' = |\vec{x} - \vec{x}'|$ on the surface plane.

Within the CWT hypothesis of independent Gaussian distributions for each ξ_q, Bedeaux and Weeks[23] got

$$\begin{aligned} P(\xi, \xi', x) &= \hat{\exp}\left[S(x)\frac{\partial^2}{\partial\xi\partial\xi'}\right]P(\xi)P(\xi') \\ &= \sum_{n=0}^{\infty}\frac{[S(x)]^n}{n!}\frac{\partial^n P(\xi)}{\partial\xi^n}\frac{\partial^n P(\xi')}{\partial\xi'^n} \end{aligned} \tag{10}$$

with the height-height correlation function

$$S(|\vec{x}-\vec{x}'|) = \langle \xi(\vec{x})\xi(\vec{x}')\rangle_\xi - \langle \xi(\vec{x})\rangle_\xi \langle \xi(\vec{x}')\rangle_\xi. \tag{11}$$

The Fourier transform of $P(\xi, \xi', x)$ is

$$P(\xi,\xi',q) = \sum_{n=0}^{\infty} \frac{S_n(q)}{n!} \frac{\partial^n P(\xi)}{\partial \xi^n} \frac{\partial^n P(\xi')}{\partial \xi'^m} \tag{12}$$

with the Fourier transform of $S(x)$ powers,

$$S_n(q) \equiv \int d\vec{x}\, S(x)^n\, e^{i\vec{q}\cdot\vec{x}}. \tag{13}$$

Replacing (12) in (9) gives

$$G_{\rm BW}(z,z';q) = \sum_{n=1}^{\infty} \frac{S_n(q)}{n!} \nu^{(n)}(z)\nu^{(n)}(z'), \tag{14}$$

where

$$\nu^{(n)}(z) = \int_{-\infty}^{\infty} d\xi \left.\frac{\partial^n \rho_{\rm I}(y)}{\partial y^n}\right|_{y=z-\xi} P(\xi) = \frac{\partial^n \rho(z)}{\partial z^n}. \tag{15}$$

Wertheim's pioneering prediction (3) corresponds to the $n = 1$ term of (14), with $S_1(q) = L_{\rm xy}^2 \langle |\xi_q|^2\rangle \equiv 1/(q^2\beta\gamma(q))$, from (1). The $n \geq 2$ terms of the series may be built from $\rho(z)$ and $\gamma(q)$, but in contrast with Wertheim's term their contribution for a given q depends on the full CW spectrum, to get $S(x)$ from $\gamma(q)$ and $S_n(q)$ through (13). This implies that the dependence of $G_{\rm BW}(z, z'; q)$ with the system size $L_{\rm xy}$ is not coming only through the dependence of the density profile $\rho(z)$ but also through the coefficients $S_n(q)$ for $n \geq 2$. That will become important when we use the CWT to extrapolate from MD boxes to experimental X-ray beam sections used in surface diffraction experiments. At the other end of the CW spectrum, the BW series depends also on its assumed molecular top, i.e., on the way in which the split average (4) is defined to separate CW from non-CW fluctuations, which needs a well-tuned choice of the ISM parameters. On top of that, a quantitative comparison of $G_{\rm BW}$ with the full density correlation G could only be done if we take out the non-CW background $G_{\rm bg}$.

C. Non-CW contributions beyond Bedeaux-Weeks theory

The split average used for the density profile in (5) and (8) may be applied to the density correlation (2) and, with the CWT assumption $\rho_{\rm I}[\vec{x}, z; \xi] \approx \rho_{\rm I}(z)$, we add and subtract equivalent terms, to get

$$\begin{aligned} G(z,z',|\vec{x}-\vec{x}'|) &\equiv \langle \hat\rho(\vec{r})\hat\rho(\vec{r}\,')\rangle - \langle\hat\rho(\vec{r})\rangle\langle\hat\rho(\vec{r}\,')\rangle \\ &\approx \Big\langle \rho_{\rm I}^{(2)}[\vec{x}, z-\xi(\vec{x}), \vec{x}', z'-\xi(\vec{x}'); \xi] \\ &\quad - \rho_{\rm I}[\vec{x}, z-\xi(\vec{x}); \xi]\, \rho_{\rm I}[\vec{x}', z'-\xi(\vec{x}'); \xi]\Big\rangle_\xi \\ &\quad + \big\langle \rho_{\rm I}(z-\xi(\vec{x}))\rho_{\rm I}(z'-\xi(\vec{x}'))\big\rangle_\xi - \rho(z)\rho(z'), \end{aligned} \tag{16}$$

with the equivalent of (6) for the "intrinsic" (shifted) two-sites density distribution as a functional of $\xi(\vec{x})$,

$$\rho_{\rm I}^{(2)}[\vec{x}, z, \vec{x}', z'; \xi] \equiv \langle \hat\rho(\vec{x}, z+\xi(\vec{x}))\hat\rho(\vec{x}', z'+\xi(\vec{x}'))\rangle_{\{\vec{r}_i\}\in[\xi]}. \tag{17}$$

$G_{\rm BW}$ in (9) and (14) is the last line in (16), so that the average in the second and third lines gives a formal expression for the non-CW background $G_{\rm bg}$, consistently with the split average used to get $\rho_{\rm I}(z)$ and $S(x)$ in BW analysis.

A MD sampling of the intrinsic two-sites density distribution functional (17) is infeasible but, as done for $\rho_{\rm I}[\vec{x}, z; \xi]$ to get (8), we assume that it is self-averaged. Then, the intrinsic density correlation,

$$G_{\rm I}(z,z',x'') = \Big\langle \rho_{\rm I}^{(2)}[\vec{x}, z, \vec{x}', z'; \xi]\Big\rangle_\xi - \rho_{\rm I}(z)\rho_{\rm I}(z'), \tag{18}$$

is used to get the (shifted) average of $\rho_{\rm I}^{(2)}$ and, from (16),

$$\begin{aligned} G_{\rm bg}(z,z',x'') &\approx \langle G_{\rm I}(z-\xi(\vec{x}), z'-\xi(\vec{x}'), x'')\rangle_\xi \\ &= \int d\xi \int d\xi' G_{\rm I}(z-\xi, z'-\xi', x'')P(\xi,\xi',x''). \end{aligned} \tag{19}$$

The average with $P(\xi, \xi', x'')$ in (9) was essential to get the CW effects for long distances x'', but it may be simplified in (19) because $G_{\rm I}(z, z, x'')$ is short-ranged in x''. Therefore, we take the $x'' = 0$ limit, $P(\xi, \xi', x'') \approx \delta(\xi - \xi')P(\xi)$, to get

$$G_{\rm bg}(z,z',x'') \approx \int d\xi\, G_{\rm I}(z-\xi, z'-\xi, x'')P(\xi). \tag{20}$$

Taking out this non-CW background gives the bare CW contribution to the density correlations,

$$\Delta G(z,z';q) \equiv G(z,z';q) - G_{\rm bg}(z,z';q), \tag{21}$$

directly from our MD simulations and consistently with the ISM definition used to get (11) and (13) for the BW prediction (14). In our previous work for the LJ surface,[30] we had defined $G_{\rm I}(z, z'; q)$ as in (18), obtained it from MD simulations, and used it as an intuitively appealing proposal for $G_{\rm bg}(z, z'; q)$. The theoretical derivation given here formalizes the concept and the convolution (20) provides the dependence of the non-CW correlation background with the system size, consistently with the density profile (8). Nevertheless, for the size of our simulation box, there would be very little change if we take $G_{\rm bg} \approx G_{\rm I}$.

III. MOLECULAR DYNAMIC SIMULATIONS

In order to check the theory of Bedeaux and Weeks, we have studied the liquid-vapor interface of two very different simple liquid models close to their triple points: the first one is the well-known Lennard-Jones (LJ) potential (truncated at $r_{\rm c} = 4.4\sigma$), with a ratio $T_{\rm t}/T_{\rm c} = 0.56$ between triple and critical T; the second model is the soft-alkali (SA) pairwise interaction potential,[31,32] with a soft repulsive core designed to give a low triple point temperature, $T_{\rm t}/T_{\rm c} = 0.10$, similar to the experimental values for some liquid metals. The low triple point temperature allows us to study a very stiff cold liquid surface, with high surface tension and very low CW amplitudes.

We used the LAMPPS package[36] to run canonical ensemble NVT-MD simulations of liquid slabs coexisting with the vapor, at kT close to the triple point temperature. For the LJ system, we use $T/T_{\rm c} = 0.63$ and a rectangular box with periodic

boundary conditions at $L_{xy} = 41.82\sigma$. The cold SA system is simulated at $T/T_c = 0.12$ and with $L_{xy} = 36.10\sigma$. The MD step is $dt = 5 \times 10^{-3}\sigma\sqrt{m/\epsilon}$, and the Nose-Hoover thermostat was set with a time constant 10 dt. For the initial configuration, we used a previously equilibrated liquid bulk in a smaller cubic box, then that box was replicated to fill a slab of thickness $3L_{xy}$, within the full simulation box, leaving initially empty a similar volume. Each system was equilibrated in 2×10^6 MD steps, to form thick liquid and vapor slabs. The thickness of the liquid slab guarantees that the CW fluctuations at the two interfaces are decoupled. We sampled 5000 configurations, separated by 5000 MD time steps. These long simulation runs are needed to get good statistics for the slow CW fluctuations with the smallest q. The same set of configurations was used to get $\beta\gamma_o\sigma^2 = 1.50 \pm 0.01$ for LJ and $\beta\gamma_o\sigma^2 = 10.71 \pm 0.02$ for SA, from the integral of the virial expression for the pressure tensor components.

As presented in Fig. 1, the main difference between the LJ (top) and the SA (bottom) surfaces is that, with our simulation boxes, $\rho(z)$ is monotonic for LJ, while the SA surface has a strong layering structure. The CWT with $\gamma(q) = \gamma_o$ may be safely used to include through (8) the CW fluctuations in a larger box, and we show the damping of the oscillatory structure in $\rho(z)$ for a SA surface[31,32] with a transverse size 32 L_{xy}. By contrast, the same increase of L_{xy} produces only a very weak broadening of the monotonic $\rho(z)$ in the LJ surface, which would be hardly visible in Fig. 2.

A. The intrinsic sampling method

The evaluation of $\xi(\vec{x})$ and $\rho_I(z)$ in computer simulations provides a direct test to the CWT assumptions, and their range of validity is shown to depend on the explicit IS definition used to split the statistical averages (4). The choice for that definition plays a role similar to that of a local order parameter in terms of the molecular configuration, to be used in a Landau-Ginzburg theory. The theoretical scheme is independent of that choice, but a good definition gives a wider range to match the molecular and the mesoscopic descriptions.

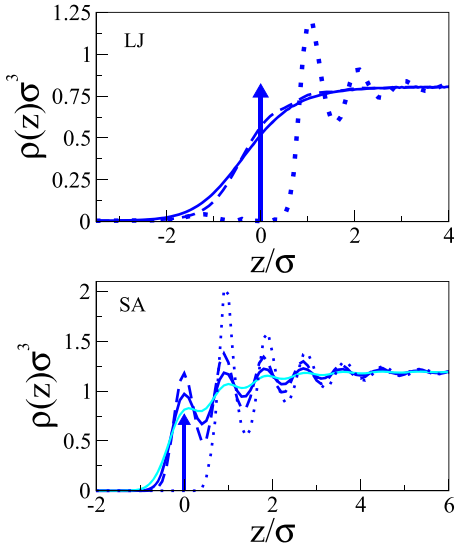

FIG. 1. MD-ISM results for the mean and intrinsic density profiles. Top panel: LJ model at $T/T_c = 0.63$ and bottom panel: SA model at $T/T_c = 0.12$. Full line: mean density profiles in the MD box; dotted line: intrinsic density profiles $\rho_I(z, q_m)$ at the sharpest resolution $q_m \simeq 2\pi/a_0$ (the vertical arrows proportional to the δ-function peak at the IS); dashed line: intrinsic density profiles at optimal resolutions for the matching with CWT, $q_m\sigma = 0.63$ for LJ and $q_m\sigma = 0.70$ for SA. In the bottom panel, the full gray (cyan) line shows the CWT prediction for the SA mean density profile in a system with a lateral size increased by a factor of 32.

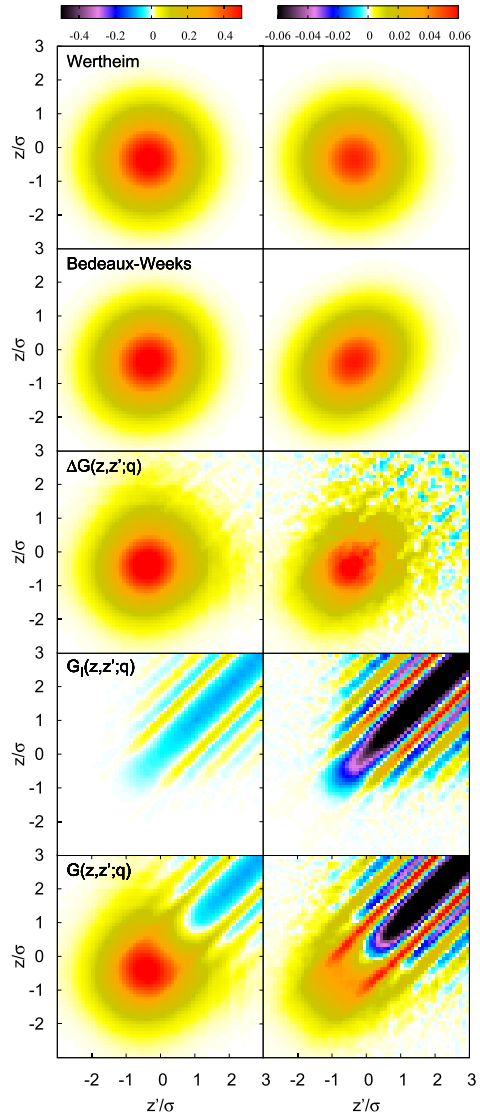

FIG. 2. Density correlation function in the LJ surface. Left column $q\sigma = 0.15$, right column $q\sigma = 0.45$. First row: Wertheim's term, i.e., $G_{BW}(z, z'; q)$ at order $n = 1$; second row: full Bedeaux-Weeks series $G_{BW}(z, z'; q)$; third row: the bare CW contribution $\Delta G(z, z'; q)$; fourth row: the intrinsic $G_I(z, z'; q)$; and fifth row: the total $G(z, z'; q)$ directly from MD, excluding the ideal self-correlation term $\rho(z)\delta(z - z')$.

The Intrinsic Sampling Method (ISM)[25,26,37] is a practical implementation of many-body definitions based on percolation analysis.[38,39] As in our previous work[30] for the LJ surface, we have applied the method to 5000 MD configurations for each model. The algorithm is fully described in Ref. 26, and we use the same parameters as in Ref. 25. The IS is represented by its Fourier components ξ_q for any wavevector $\vec{q} = 2\pi(n_x, n_y)/L_{xy}$ with integer $n_{x,y}$ and $\xi_0 \equiv \langle\xi(\vec{x})\rangle = 0$ as the origin for z. The upper wavevector limit, $|q_x|, |q_y| \le q_m$, controls how closely

the mathematical surface $z = \xi(\vec{x})$ follows the molecular positions, and the intrinsic profile has a parametric dependence on it. In Fig. 1 we present, together with the mean density profiles, the intrinsic profiles (7) for the LJ and SA surfaces. At the maximum resolution, $q_m = 2\pi/a_0$ (in terms of the intermolecular distance a_0), $\rho_I(z; q_m)$ has a delta-function peak (vertical arrows) at $z = 0$, as the molecular occupancy on the IS, and a strong layering at the liquid side. At that maximum resolution of the method, the CWT assumptions leading to (8) are not fulfilled,[37] but decreasing the value of the parameter q_m allows us to move gradually to the CWT range of validity. The intrinsic profiles that we have used to test the G_{BW} series are also presented in Fig. 2. For the LJ system, ($q_m = 0.63/\sigma$) gives already a nearly monotonic density profile although some oscillatory structure is observed in the derivative (not shown here). For the SA surface, the ISM intrinsic profile with $q_m = 0.70/\sigma$ is still strongly layered and qualitatively different from the empirical monotonous shapes assumed in the theoretical analysis of the CWT predictions,[23] but similar to those inferred from the X-ray reflectivity data on cold liquid metal surfaces.[33,34]

IV. THE DENSITY CORRELATION FUNCTION

A. MD results for G(z, z′; q)

The transverse Fourier transform of (2), for $q \neq 0$,

$$G(z, z'; q) = \left\langle \sum_{i,j=1}^{N} \frac{e^{i\vec{q}\cdot\vec{x}_{ij}}}{L_{xy}^2} \delta(z - z_i)\delta(z' - z_j) \right\rangle \qquad (22)$$

was averaged as a (z, z') matrix with binning $\Delta z = \sigma/10$. The statistics from the two interfaces of the slab was accumulated, with z and z' referred to the instantaneous dividing plane at each interface, to get $\xi_0 = 0$. The bottom rows in Figs. 2 and 3 present $G(z, z'; q)$ for LJ and SA, respectively, excluding the ideal self-correlation term $\rho(z)\delta(z - z')$ given by $i = j$ in (22). The left columns correspond to the lowest q within our simulation box, $q = 2\pi/L_{xy}$; the right column is for q three times larger. In the LJ surface (Fig. 2) at the lowest q, the CW contribution proportional to $\rho'(z)\rho'(z')/q^2$ (shown in the top frame) appears strong and clear in the full $G(z, z'; q)$ as a round maximum at the middle of the interface. Toward the vapor ($z, z' < 0$), the correlation dies out of the CW peak, while toward the liquid, we observe the typical oscillatory correlation in a dense liquid, which depends on $|z - z'|$ as shown by the diagonal bands. In the right column, the q^{-2} dependence of Wertheim's CW peak reduces it by a factor of 9 with respect to the left column; the change of scale makes more visible the layering structure, which in the liquid side is essentially independent of q and dominates $G(z, z'; q)$ for $z, z' \gtrsim \sigma$. The surface layering in the SA model (bottom panels of Fig. 3) gives a very different density correlation. At the lowest q, the CW contribution is also dominant, but instead of the round maximum of the LJ system, we observe a checkerboard structure produced by the alternating sign of $\rho'(z)\rho'(z')$. On top of it, we observe the non-CW contribution, with diagonal bands similar to that of the LJ, whose relative weight increases with q.

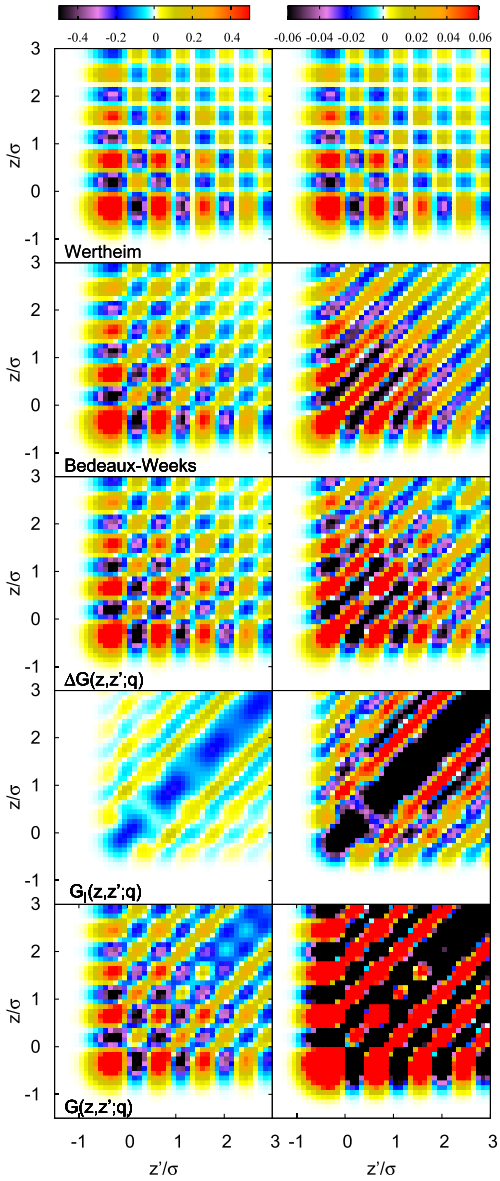

FIG. 3. Density correlation function in the SA surface. Left column $q\sigma = 0.174$, right column $q\sigma = 0.522$. First row: Wertheim's term, i.e., $G_{BW}(z, z'; q)$ at order $n = 1$; second row: full Bedeaux-Weeks $G_{BW}(z, z'; q)$; third row: the bare CW contribution $\Delta G(z, z'; q)$; fourth row: the intrinsic $G_I(z, z'; q)$; and fifth row: the total $G(z, z'; q)$ directly from MD excluding the ideal self-correlation term $\rho(z)\delta(z - z')$.

B. The intrinsic and non-CW background correlations

The Fourier transform of the intrinsic density correlation (18), $G_I(z, z'; q)$, is obtained changing z_α ($\alpha = i, j$) in (22) by $z_\alpha - \xi(\vec{x}_\alpha)$, with the IS obtained from the molecular positions in each sampled MD configuration.[30] $G_I(z, z'; q)$, as $\rho_I(z)$, does not depend on L_{xy}, but it depends on the ISM parameters used to define $\xi(\vec{x})$ from the molecular positions, the most relevant being the upper wavevector cutoff q_m. An IS defined to follow very closely the LJ molecular positions, $q_m \simeq 2\pi/a_0$, eliminates from G_I not only the CW but also some non-CW fluctuations.[30] Decreasing q_m, we reach a rather broad range for this parameter in which $G_I(z, z'; q)$ takes the expected aspect of strong layering, depending on $|z - z'|$ and weighted by the product of the intrinsic profiles

$\rho_I(z)\rho_I(z')$. If we keep reducing the value of q_m beyond that range the CW fluctuations with $q > q_m$ are included in G_I as they are in G so that these CW fluctuations are eliminated in ΔG.

The fourth rows in Figs. 2 (LJ) and 3 (SA) show $G_I(z, z'; q)$ with the optimal choice $q_m\sigma = 0.63$ for the LJ and 0.70 for the SA, respectively. In both liquid surfaces, the effects of the CW fluctuations in $G(z, z'; q)$ have disappeared in $G_I(z, z'; q)$, although the layering in Fig. 3, the SA surface shows up as a structure along the main diagonal.

The probability distribution $P(\xi)$ obtained along the same MD-ISM is used to get the non-CW background of the density correlation G_{bg} in (19) which, as the full G and the density profile, depends on the system size. The ideal-gas self-correlation [i.e., the $i = j$ terms in (22)] is exactly equal in (19) so that it is fully eliminated in the bare CW contribution ΔG in (21).

C. Bedeaux-Weeks series for the density correlation

From the MD-ISM, we get $\langle|\hat{\xi}_q|^2\rangle$ or equivalently through (1) $\gamma_{ISM}(q)$. The height correlation $S(x) = \sum_{q\neq 0}\langle|\hat{\xi}_q|^2\rangle e^{i\vec{q}\vec{x}}$ is directly obtained, and it shows the predicted long range decay $S(x) \sim -\log(x/L_{xy})$ for $2\pi/q_m \ll x \ll L_{xy}$, associated with the $S_1(q) \sim q^{-2}$ behavior at low q. The coefficients $S_n(q)$ for $n \geq 2$ in the BW series (14) are obtained through numerical Fourier transform of $S(x)$ powers, and they have a finite $q = 0$ limit, i.e., they do not contribute to the long-range decay of $G_{BW}(z, z'; q)$, but still they can give an important contribution which, in contrast to $S_1(q)$ in Wertheim's term, grows with the sampled area.

The converge of BW series had been theoretically explored under simple theoretical assumptions for the CW spectrum and the intrinsic profile.[40] Here we explore it with $\langle|\xi_q|^2\rangle$ and $\rho(z)$ directly obtained from MD simulations, with the ISM optimized to define $\xi(\vec{x})$ from the molecular positions. The top panels in Figs. 2 and 3 show Wertheim's ($n = 1$) contribution and below them the full BW series. For the lowest q in the LJ surface (Fig. 2), the $n = 1$ term gives most of the structure in $G_{BW}(z, z'; q)$, while at larger q, there are small contributions of $n \geq 3$, which break the perfect factorization $\rho'(z)\rho'(z')$ of Wertheim's prediction. The cold SA liquid has a much stiffer surface, with $\beta\gamma_o\sigma^2 = 10.5$ versus 1.5 for the LJ liquid. Assuming a monotonic intrinsic density profile (as done in the original BW analysis[23]) that would imply a much reduced effect of the $n \geq 2$ terms in the $G_{BW}(z, z'; q)$ series for the SA surface. However, as shown in Fig. 1, the intrinsic profiles at the maximum resolution of the ISM are strongly layered (both for LJ and SA); the stiffness of the cold liquid interface keeps an oscillating tail in the SA density profile, while the larger CW amplitude in the LJ system erases the molecular packing effects in $\rho(z)$ for similar sizes of the MD box. The higher order derivatives of the SA profile reflect that oscillating structure and grow fast (in absolute value) with the order n. Therefore, for the SA interface (Fig. 3), the $n > 1$ terms are visible for the lowest q and very strong for q three times larger. In practice, we had to add up to $n = 7$ to get no visible changes in the figure. The main effect of the $n \geq 2$ terms it is to introduce in $G_{BW}(z, z'; q)$ a (local-like) dependence on $|z - z'|$, as that from the background correlations, but which arises entirely from CW fluctuations.

D. The bare CW density correlation

The third rows in Figs. 2 and 3 show the bare CW contribution (21), taking the non-CW background out of the full density correlation G. In the LJ surface (Fig. 2), the round CW peak in $G(z, z'; q)$ is perfectly well reproduced by $\Delta G(z, z'; q)$ and the diagonal oscillatory tail, from the dense liquid correlations, is eliminated. The cold SA liquid (Fig. 3) shows strong surface layering but it is still clear that $\Delta G(z, z'; q)$ extracts the CW peak, nearly clean of non-CW correlations, even when the latter dominate the total $G(z, z'; q)$.

We have now two complementary routes to get the CW contribution to the density correlation. One is the G_{BW} series built with $\rho(z)$ and $S(x)$ obtained from the MD-ISM; the other is the bare CW correlation ΔG, obtained from the full G in (2) and (22) and with our proposal for the non-CW background (19). The visual agreement between their representations in the second and third rows of Figs. 2 and 3 is complemented by a more quantitative assay in Sec. V, as well as for the relevance of taking the full BW series, rather than Wertheim's ($n = 1$) term.

V. DISCUSSION

Wertheim's analysis (3) implies that for very small q the CW fluctuations give the eigenmode of the density correlation with the largest eigenvalue $\lambda_0(q) \sim q^{-2}$, and with eigenfunction $\langle z|\mathrm{CW}\rangle$ very close to $\rho'(z)$. In a previous study,[30] following an early proposal by Stecki,[18] we had proposed to diagonalize $\Delta G(z, z'; q)$ [or $G(z, z'; q)$] as the best way to get the bare (or dressed) CW representation. The "normal mode" surface tension was defined (in the usual bra-ket notation) as

$$\beta\gamma_{NM}(q) \equiv \frac{\langle\rho'|\rho'\rangle}{q^2\lambda_0(q)} = \frac{\langle\rho'|\rho'\rangle}{q^2}\frac{\langle \mathrm{CW}|\mathrm{CW}\rangle}{\langle \mathrm{CW}|\Delta G|\mathrm{CW}\rangle} \approx \frac{\left[\int dz\ \rho'(z)^2\right]^2}{q^2\int dz\int dz'\rho'(z)\Delta G(z, z'; q)\rho'(z')}. \quad (23)$$

That amounts to consider the first term in (3) as the full CW contribution, i.e., to define the "regular terms" as any contribution orthogonal to $|\rho'\rangle$, as proposed by Blokhuis *et al.*[13,14] Our previous analysis of the LJ surface gave a very good agreement between $\gamma_{NM}(q)$ and the direct ISM result $\gamma_{ISM}(q)$ obtained through (1).

In Fig. 4, we use (23) with BW series instead of ΔG, to show the effect of truncating (14) at different orders. Wertheim's ($n = 1$) term alone gives back precisely the surface tension $\gamma_{ISM}(q)$ used as an input and represented by the continuous lines. Adding $n = 2$ does not change it because $\rho''(z)$ is orthogonal to $\rho'(z)$, but extending the BW series to $n \geq 3$ gives both a quantitative assay for the convergence of the series and a measure of the error made when Wertheim's term is considered the only CW contribution to the pair correlation.

In the LJ surface (with our simulation box), the $n = 3$ contribution is visible but small, and higher orders are negligible. As obtained in our previous study,[30] the result $\gamma_{NM}(q)$

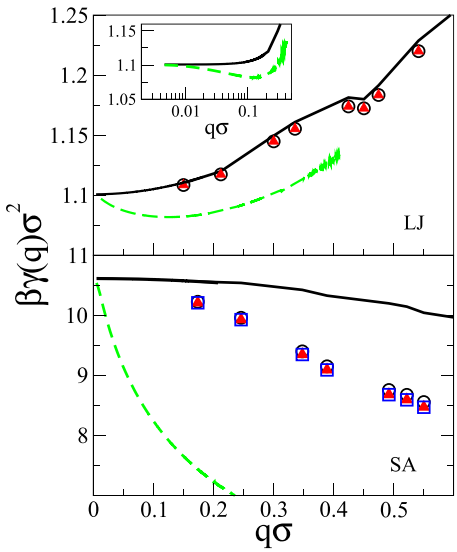

FIG. 4. The adimensional $\beta\gamma_{\rm NM}(q)\sigma^2 \equiv \frac{\langle\rho'|\rho'\rangle}{(q/\sigma)^2\lambda_0(q)}$ from (23), with Bedeaux-Weeks series, $G_{BW}(z, z'; q)$, truncated at different orders, for LJ (top) and SA (bottom). Full line (black) $n = 1$, circles (black) $n \le 3$, triangles (red) $n \le 5$, and squares (blue) $n \le 7$. The dashed line (green) indicates the theoretical prediction for the $G_{BW}(z, z'; q)$ for a system with a lateral size 32 times that of the present simulation. The inset in the top panel shows the LJ results with log-scale for q, which as used in Ref. 7 to represent the analysis of experimental data.

$\approx \gamma_{\rm ISM}(q)$ indicates that with a good representation of the non-CW contributions, as the only "regular terms" in $G(z, z'; q)$, Wertheim's prediction (3) could be safely used to get $\gamma(q)$ in agreement with its direct (ISM) evaluation. By contrast, the layered $\rho(z)$ in the cold SA surface enhances the $n = 3$ contribution and gives $\gamma_{\rm NM}(q)$ well below the input $\gamma_{\rm ISM}(q)$. We could still discern the contributions up to $n = 7$, but they have a minor effect. We know that these high n terms in the BW series are still pure CW contributions to the density correlations and the difference between the estimated $\gamma_{\rm NM}(q)$ and the direct ISM result gives the error made when the full CWT prediction (14) is interpreted as (3), as it has been often done in the analysis of experimental and computer simulation results.

The main advantage of a good quantitative matching between MD-ISM and CWT is that we may use the latter, on its safe side, to extrapolate the density correlations to $L_{\rm xy}$ much larger than the simulation box, as done in Fig. 1 for $\rho(z)$. That is crucial for the interpretation of experimental X-ray diffraction data, which sample the liquid surface over the section of the beam, with $L_{\rm xy}$ of the order of a micrometer. Within the interpretation of the CW signal as the $n = 1$ term of BW series the only effect of increasing $L_{\rm xy}$ is to make accessible a finer mesh and smaller values of q. The continuous (black) lines in Fig. 4 correspond to the interpolation/extrapolation of $\gamma_{\rm ISM}(q)$ from our MD box to $L_{\rm xy} = 1338.24\sigma$. This extended $\gamma_{\rm ISM}(q)$ is used in (1) and (8) to get the (slightly smoother) mean density profile and in (14) to get $G_{\rm BW}(z, z'; q)$ for that large $L_{\rm xy}$. The dashed (green) lines give the result of (23) with this full BW series in the large box, and it is now well below the actual $\gamma_{\rm ISM}(q)$, in contrast to what was observed in our MD box. Therefore, the interpretation of the largest eigenvalue of $G_{\rm BW}(z, z'; q)$ as its $n = 1$ term would produce a gross underestimation of $\gamma(q)$ not only in the cold SA liquid surface but also in the typical simple liquid surface represented by the LJ model, when $L_{\rm xy}$ is large. The inset shows $\gamma_{\rm ISM}(q)$ and $\gamma_{\rm NM}(q)$ with log-scale for q, as used in Fig. 4 of Mora *et al.*[7] to represent the inferred $\gamma(q)$ for several molecular liquids, which give qualitatively similar shapes. The apparent reduction of the surface tension with increasing q, which had also been reported for water,[41] was interpreted as an effect of long-range dispersion forces.[11] That interpretation had been questioned by two of us on the basis of an ISM analysis,[42] and the present results suggest an alternative explanation, the role of the higher order terms in Bedeaux-Weeks series when they are forced into the functional form of Wertheim's prediction. The depth of the minimum in $\gamma_{\rm NM}(q)$ could be increased just considering larger $L_{\rm xy}$.

To get a quantitative comparison between $G_{\rm BW}(z, z'; q)$ and $\Delta G(z, z'; q)$ for any q, we may use their projections on the (non-orthogonal) basis given by the n-th order derivatives of the density profile. Truncating the basis to $n \le m$, we define the symmetric $m \times m$ matrices A and B, with elements

$$A_{i,j} = \langle\rho^{(i)}|\rho^{(j)}\rangle, \text{and} \quad B_{i,j} = \langle\rho^{(i)}|\Delta G|\rho^{(j)}\rangle. \tag{24}$$

The equivalent matrix $B^{\rm BW}$ from the projections of $G_{\rm BW}(z, z'; q)$ (15) may be written as $B^{\rm BW} = AC^{\rm BW}A$, for a diagonal matrix with $C^{\rm BW}_{n,n} = S_n(q)/n!$. The inverse matrix A^{-1} may be used to get $C^{\rm BW} = A^{-1}B^{\rm BW}A^{-1}$, so that $C^{\rm BW}_{1,1} = S_1(q) = 1/(q^2\beta\gamma_{\rm ISM}(q))$, when BW series is built on the ISM result for $S(x)$. Then we may assume the same deconstruction applies to (24) and get the matrix $C = A^{-1}BA^{-1}$ that describes ΔG, to extract from its (1, 1) element a deconstructed (dc) surface tension function

$$\gamma_{\rm dc}(q) \equiv \frac{kT}{q^2 C_{1,1}} = \frac{kT}{q^2 \sum_{i,j} A^{-1}_{1,i} B_{i,j} A^{-1}_{j,1}}. \tag{25}$$

As shown in the upper panel in Fig. 5, for the LJ surface in our MD box we get $\gamma_{\rm c}(q) \approx \gamma_{\rm NM}(q) \approx \gamma_{\rm ISM}(q)$ since Wertheim's term is the only relevant contribution to BW series and we had already probed its accuracy describing the bare CW contribution ΔG. By contrast, for the SA surface in the lower panel of the figure, the NM hypothesis (23) applied to ΔG gives a result as poor as when applied to $G_{\rm BW}$ in Fig. 4, but the deconstruction procedure gives back a $\gamma_{\rm dc}(q)$ quite close to the $\gamma_{\rm ISM}(q)$ direct result. We have used truncations up to $m = 7$, but $m = 3$ already gives most of the effect.

We include in Fig. 5 the NM results from the total $G(z, z'; q)$ which, as already shown in our previous work[30] for the LJ surface, gives a very flat $\gamma_{\rm NM}(q) \approx \gamma_o$ up to a sharp physical cutoff $q_u \approx 0.3/\sigma$ at which the CW mode merges into the band of non-CW fluctuations. That is represented in the figure by the result of (23) with the largest eigenvalue of $G_{\rm bg}$. The relevance of the $n \ge 2$ terms in BW series for the cold SA surface produces very different results. The NM result for the "dressed" CW in the full $G(z, z'; q)$ produces a $\gamma(q)$ which is quite below that for the bare CW in ΔG, which were already well below $\gamma_{\rm dc}(q) \approx \gamma_{\rm ISM}(q)$. That makes clear the relevance of taking into account both the non-CW background and the $n \ge 2$ terms of BW series in any attempt to "read" the CW spectrum in this cold liquid surface, even within the limits of our MD simulation

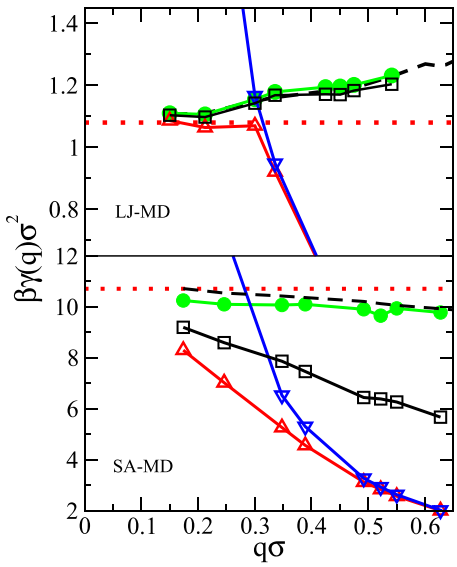

FIG. 5. The adimensional $\beta\gamma_{NM}(q)\sigma^2 \equiv \frac{\langle\rho'|\rho'\rangle}{(q\sigma)^2\lambda_0(q)}$ from (23), for the LJ (top) and SA (bottom) surfaces. Empty symbols are $\gamma_{NM}(q)$ from the eigenvalues of the bare density correlation $\Delta G(z, z'; q)$ (black squares), of the total $G(z, z'; q)$ (red up-triangles), and of the non-CW background correlation $G_{bg}(z, z'; q)$ (blue down-triangles). The latter should not be interpreted as a surface tension since G_{bg} has no CW term at all, but it is presented to show its merging with the results from the total G at large q. Full green circles are the deconstructed $\gamma_{dc}(q)$ from (25). The black dashed line is the direct ISM results for $\gamma(q)$, and the red dotted line is the virial surface tension γ_o.

box. These two contributions are entangled, since the layering structure at the surface produces a strong hybridization of the CW fluctuations with the bulk-like fluctuations in G_{bg}, and that produces the smooth merging of the highest eigenvalues of G and G_{bg} in contrast with their sharp crossing for the LJ fluid. The possible application to the full G of the deconstruction procedure for $\gamma_{dc}(q)$, as applied to ΔG, is not explored here.

VI. CONCLUSIONS

The main conclusion of the present work is that Bedeaux-Weeks theory for the capillary wave effects on the density correlations at a liquid surface is both quantitatively accurate and needed since Wertheim's ($n = 1$) term does not give a full account of those effects. The good agreement between the bare CW contribution, defined with our approximation for the non-CW background (19), strongly supports BW analysis within the CWT and our proposal for G_{bg}, using the MD-ISM results to close the circle in opposite directions and to meet each other, $G_{BW} \approx \Delta G$, with high quantitative accuracy.

The results for the cold SA surface make clear the need of the full G_{BW} series, rather than Wertheim's proposal which has been systematically used in the attempts to extract an extended surface tension $\gamma(q)$ from surface diffraction experiments, MD simulations, and DF theories. The strong surface layering of the cold SA surface is similar to that observed in X-ray diffraction of liquid metal surfaces[33,34] and enhances the role of the higher order derivatives of the density profile in BW series. The MD results for the LJ surface (or, those not shown here for the SA model at higher temperature) with monotonous density profiles may suggest that Wertheim's analysis is good enough; however, even in those systems the terms $n \geq 3$ in BW series become important when the liquid surface is sampled over larger areas, as those set by the X-ray beams with L_{xy} of several hundreds of molecular diameters. Therefore we have to question the analysis of experiments done under the assumption that all the "regular terms" in (3) could be extracted as non-CW fluctuations. In fact, the shape of $\gamma(q)$ extracted from some experimental data looks very similar to what we get in Fig. 4 when the full G_{BW} series is analysed as being given by Wertheim's functional form.[7,41]

Although the higher order terms in BW series force us to use a more cumbersome analysis, from the full access to the bare CW contribution $\Delta G(z, z'; q)$, we may accurately deconstruct the series and recover the $\gamma_{ISM}(q)$ used as a molecular input into the CWT to get $G_{BW}(z, z'; q)$. Therefore, we confirm a main conclusion of our previous work, i.e., after taking out the non-CW background in $G(z, z'; q)$, the two-particle correlation $\Delta G(z, z'; q)$ contains the relevant information to extract a $\gamma(q)$, very close to that given by the $N-$particle percolation analysis of the ISM with optimized parameters, and which may be regarded as a good physical representation for the bare CW fluctuations.

Such deconstruction of $\gamma(q)$ appears infeasible from the much more limited access to the density correlations provided by X-ray diffraction, giving the surface structure factor, i.e., the integral of $G(z, z'; q)$ over z and z' through the X-ray penetration region, and with the off-specular signal as a way to extract the non-CW background. It is important to realize that the success of the simpler normal mode analysis (i.e., the irrelevance of the $n > 1$ terms in BW series) for the LJ surface applies only over a restricted Wertheim's window for the system size $10\sigma \lesssim L_{xy} \lesssim 100\sigma$, such that it allows enough CW broadening of the intrinsic profile to give smooth $\rho(z)$ in the simulation box, but still keeps low contributions from the higher $S_n(q)$ terms in BW series. Wertheim's window is closed (or shifted to computationally unreachable large sizes) in the cold SA surface that probably is a qualitatively good representation of more realistic liquid metal surface simulations with respect to the CW effects.

A key point to achieve the good matching between ΔG and G^{BW} is the definition of the intrinsic surface shape from the molecular positions. The ISM defines $\xi(\vec{x})$ in a way that separates (as much as possible) the fluctuations in the shape of the IS from the density fluctuations measured on that surface, and that provides a clear cut distinction between the bare and dressed CW fluctuations.[30] Within the theoretical formalization in Sec. II, that separation between the IS undulations and the instantaneous density on that surface [i.e., $\hat{\rho}(\vec{x}, z)$ for $z = \xi(\vec{x})$] corresponds to make as good as possible the CWT assumption of self-averaging for the intrinsic density $\rho_I[\vec{x}, z; \xi] \approx \langle\rho_I[\vec{x}, z; \xi]\rangle_\xi \equiv \rho_I(z)$. However, the N-particle percolation analysis used by the ISM implies to know the molecular structure far beyond what is accessible in experiments, as it extracts from MD simulations a large amount of information that is discarded in the traditional one-site (density profiles) and two-site (correlations) averages.

We may conclude that the quantitative matching between the molecular description of liquid surfaces in computer

simulations and their mesoscopic analysis within the CWT has been fully achieved, the key point being a sound and computable definition for the intrinsic surface shape from the molecular positions. We had first tried simpler proposals, like a local Gibbs-surface balance in the number of particles within narrow prisms,[22] but they cannot efficiently separate CW from bulk-like fluctuations in the liquid.[37] Stillinger's early idea of a percolation based definition[38] was finally implemented with the ISM and similar percolation-based methods, at a higher but (nowadays) affordable computational cost. The ISM allows us to extract from MD simulations the intrinsic profile, the intrinsic non-CW correlation and the function $\gamma(q)$ that consistently represent the CW spectrum because (with the choice of its internal parameters) it achieves an optimized separation between the CW of the interface and the local density fluctuations controlled by the compressibility of the liquid. With that, we may safely use the CWT to predict the correlation structure in much larger systems or limited only by the Earth gravity. The connection with density functional theories is still not so well established, although all the results presented here add support to the main line of convergence. The optimal wavevector used to define the non-CW background corresponds to set a limit of $2\pi/q_m \approx 10\sigma$ for the shortest capillary wavelengths that could be included within the framework of the CWT, and a DF approximation with a good description of the non-local effects of the molecular packing may be assumed to give a fair quantitative description of the density correlations up to that wavelength. The suggestion is that $\rho_{\mathrm{DF}}(z)$ should be interpreted as the mean density profile of the liquid surface with an effective transverse size L_{DF}, or equivalently[4] as the intrinsic profile $\rho_{\mathrm{I}}(z, q_m)$ used here to connect MD-ISM and the CWT. We may add now a similar interpretation for the correlation function $G_{\mathrm{DF}}(z, z'; q)$ as a representation of $G_{\mathrm{bg}}(z, z'; q)$. However, the validity of these interpretations should be established in the context of the different levels of approximation that are included in the generic DF formalism.

ACKNOWLEDGMENTS

We acknowledge the support of the Spanish Secretariat for Research, Development, and Innovation (Grant Nos. FIS2017-86007-C3 and FPU2015/0248) and from the Maria de Maeztu Programme for Units of Excellence in R&D (No. MDM-2014-0377).

[1] F. P. Buff, R. A. Lovett, and F. H. Stillinger, Phys. Rev. Lett. **15**, 621 (1965).
[2] R. Evans, Adv. Phys. **28**, 143 (1979).
[3] J. K. Percus and G. Williams, in *Fluid Interfacial Phenomena*, edited by C. Croxton (John Wiley, New York, 1986), pp. 1–44.
[4] E. Tarazona, P. Chacón, and F. Bresme, J. Phys.: Condens. Matter **24**, 284123 (2012).
[5] P. S. Pershan, Colloids Surf., A **171**, 149 (2000).
[6] P. S. Pershan, J. Phys. Chem. B **113**, 3639 (2009).
[7] S. Mora, J. Daillant, K. R. Mecke, D. Luzet, A. Braslau, M. Alba, and B. Struth, Phys. Rev. Lett. **90**, 216101 (2003).
[8] D. X. Li, B. Yang, B. H. Lin, M. Meron, J. Gebhardt, T. Graber, and S. A. Rice, Phys. Rev. Lett. **92**, 136102 (2004).
[9] M. Napiórkowski and S. Dietrich, Phys. Rev. E **47**, 1836 (1993).
[10] S. Dietrich and M. Napiórkowski, Phys. Rev. A **43**, 1861 (1991).
[11] K. R. Mecke and S. Dietrich, Phys. Rev. E **59**, 6766 (1999).
[12] F. Höfling and S. Dietrich, Europhys. Lett. **109**, 46002 (2015).
[13] E. M. Blokhuis, J. Kuipers, and R. L. C. Vink, Phys. Rev. Lett. **101**, 086101 (2008).
[14] E. M. Blokhuis, J. Chem. Phys. **130**, 014706 (2009).
[15] E. Chacón and P. Tarazona, J. Phys.: Condens. Matter **28**, 244014 (2016).
[16] F. Sedlmeier, D. Horinek, and R. Netz, Phys. Rev. Lett. **103**, 136102 (2009).
[17] E. Chacón and P. Tarazona, J. Phys.: Condens. Matter **17**(45), S3493 (2005).
[18] J. Stecki, J. Chem. Phys. **107**, 7967 (1997).
[19] A. O. Parry, C. Rascón, G. Willis, and R. Evans, J. Phys.: Condens. Matter **26**, 355008 (2014).
[20] A. O. Parry, C. Rascon, and R. Evans, Phys. Rev. E **91**, 030401(R) (2015).
[21] J. Hernández-Muñoz, E. Chacón, and P. Tarazona, Phys. Rev. E **94**, 062802 (2016).
[22] J. D. Weeks, J. Chem. Phys. **67**, 3106 (1977).
[23] D. Bedeaux and J. D. Weeks, J. Chem. Phys. **82**, 972 (1985).
[24] P. Tarazona and E. Chacón, Phys. Rev. B **70**, 235407 (2004).
[25] E. Chacón, E. M. Fernández, D. Duque, R. Delgado-Buscalioni, and P. Tarazona, Phys. Rev. B **80**, 195403 (2009).
[26] F. Bresme, E. Chacón, and P. Tarazona, Phys. Chem. Chem. Phys. **10**, 4704 (2008).
[27] M. Jorge, G. Hantal, P. Jedlovszky, and N. Cordeiro, J. Phys. Chem. C **114**, 18656 (2010).
[28] A. Willard and D. Chandler, J. Phys. Chem. B **114**, 1954 (2010).
[29] D. Zhukhovitskii, J. Chem. Phys. **125**, 234701 (2007).
[30] J. Hernández-Muñoz, E. Chacón, and P. Tarazona, J. Chem. Phys. **148**, 084702 (2018).
[31] E. Chacón, M. Reinaldo-Falagán, E. Velasco, and P. Tarazona, Phys. Rev. Lett. **87**, 166101 (2001).
[32] E. Velasco, P. Tarazona, M. Reinaldo-Falagán, and E. Chacón, J. Chem. Phys. **117**, 10777 (2002).
[33] B. Ocko, M. Regan, K. Penanen, P. S. Pershan, and M. Deutsch, Phys. Rev. Lett. **74**, 4444 (1995).
[34] P. Pershan, J. Appl. Phys. **116**, 222201 (2014).
[35] M. S. Wertheim, J. Chem. Phys. **65**, 2377 (1976).
[36] S. Plimpton, J. Comput. Phys. **117**, 1 (1995).
[37] E. Chacón and P. Tarazona, Phys. Rev. Lett. **91**, 166103 (2003).
[38] F. H. Stillinger, J. Chem. Phys. **76**, 1087 (1982).
[39] F. H. Stillinger and J. Weeks, J. Chem. Phys. **99**, 2807 (1995).
[40] J. Weeks, W. Saarloos, D. Bedeaux, and E. Blokhuis, J. Chem. Phys. **91**, 6494 (1989).
[41] C. Fradin, A. Braslau, D. Luzet, D. Smilgles, M. Alba, N. Boudet, K. Mecke, and J. Daillant, Nature **403**, 871 (2000).
[42] E. Chacón, E. Fernández, and P. Tarazona, Phys. Rev. E **89**, 042406 (2014).